The Ultra–Wide Bandwidth Outdoor Channel: From Measurement Campaign to Statistical Modelling

Marco Di Renzo, Fabio Graziosi, Fortunato Santucci
Department of Electrical Engineering
and Center of Excellence DEWS
Monteluco Roio 67040, L'Aquila, Italy
Email: {mdirenzo, graziosi, santucci}@ing.univaq.it

Riccardo Minutolo, Mauro Montanari
THALES ITALIA S.p.A. – Communications Division
Via E.Mattei 20, 66013 Chieti Scalo (CH), Italy
Email: Riccardo.MINUTOLO@it.thalesgroup.com
and Mauro.MONTANARI@it.thalesgroup.com

***Abstract*— This paper proposes an investigation of propagation behaviour of Ultra–Wide Bandwidth (UWB) signals in outdoor environments. Specifically, we first report on the results of an extensive measurement campaign that we have carried out in three selected scenarios, namely "forest", "hilly" and "sub–urban" environments. Then, we present the statistical model that we have derived after post–processing of collected samples by the CLEAN algorithm. While an extensive collection of results is provided in the paper, the main achievements can be summarized as follows: i) the path–loss exponent varies from 2 to 3.5 and depends on the height of transmission and reception equipments with respect to the ground floor, ii) the local mean experiences a Log–Normal shadowing with a standard deviation that may depend on the azimuth position, iii) the statistics of the first received echo in the small–scale analysis follow a Log-Normal distribution as well; iv) the delay spread in the small–scale multipath scenario results to be quite small (i.e. roughly 10ns in the forest scenario).**

I. Introduction

Ultra Wide Band (UWB) [1] is an emerging wireless technology, that is referred to as "baseband", "impulse" or "carrier–free", and it has been proposed for unlicensed operations over bandwidths spanning several GHz, provided that the power spectral density of transmitted signals is adherent to some emission masks (e.g. as specified by the Federal Communication Commission in the USA) suggested by coexistence issues with other systems [2]. A typical UWB signal [3] is composed by a sequence of ultra short pulses, whose extremely large bandwidth may enhance the capability of receivers to distinguish eventual replicas due to multipath propagation in the dispersive wireless medium. Proper combining yields reduction of fading severity, as evidenced in e.g. [4]–[6] with reference to indoor scenarios. Relevant issues, such as multiple access performance (e.g. [7]) and receiver architecture design (e.g. [8]–[12] for autocorrelation receivers based on transmitted–reference or differential approaches), have been addressed in recent literature.

Due to its extreme flexibility, UWB is currently considered by the research community worldwide for many applications, ranging from short range/high rate data communications in WPAN (*IEEE 802.15.3 Working Group*) to low–cost/low–power networking in wireless sensor networks (*IEEE 802.15.4 Working Group*). An objective of the Working Groups activity consists in selection of appropriate models for the UWB propagation channel, to be adopted for performance evaluation of transmission schemes. In fact, accurate channel characterization is vital for UWB transceiver design and for an efficient utilization of system resources (such as frequency spectrum and transmit power), as the propagation channel may pose fundamental limits to the performance of any wireless system. Due to the particular format of the transmitted signal (pulses), the richness of multipath components requires specific characterization of the propagation environment. Final recommendations of the channel model proposed by sub–committees IEEE 802.15.3a and IEEE 802.15.4a capture both the path–loss and multipath characteristics of "typical" environments, where the devices are expected to operate [13], [23]. The models considered by the sub–committees are mainly related to indoor scenarios, while existing models for outdoor environments cover only specific rural terrain [14] and suburban–like microcell scenario with a rather small range [24], [25].

Moving from these considerations and taking into account the approaches proposed in recent literature for indoor [15]–[20] and outdoor [23]–[25] propagation, we have carried out an extensive measurement campaign and derived a statistical model for three outdoor scenarios: i) forest scenario, ii) hilly terrain and iii) sub–urban scenario. Furthermore, we have been also interested on another quite unexplored aspect, i.e. propagation through a variety of materials that constitute buildings and walls (e.g. in an outdoor–to–indoor environment with and without windows). The combined consideration of these two aspects leads to model the UWB channel by a cascade of two linear (eventually time–variant) systems, that accounts for the two aspects mentioned above.

Due to the relevant complexity and variety of the wireless context, this paper resorts to a statistical approach to channel modelling and, in particular, it provides a detailed analysis of three types of effects, which are typically encountered [18], [21]: i) large–scale variations (i.e. path–loss), ii) mid–scale variations (i.e. shadowing) and iii) small–scale variations (i.e. multipath). The experimental data have been collected through a pair of commercial UWB transceivers developed by Time Domain Corporation and post–processed through the CLEAN de–convolution algorithm [19]. The "cleaned" waveforms have been used to extract some parameters and functions typically considered to characterize the channel behaviour (e.g. Mean Excess delay, Root Mean Square delay, Multipath Intensity Profile, Multipath statistics, Path–Loss vs. distance and Tx–Rx height with respect to the ground), following an approach similar to the one described in [15] and [21].

The remaining of the paper is organized as follows. In Section II, the UWB experimental propagation setup is presented.

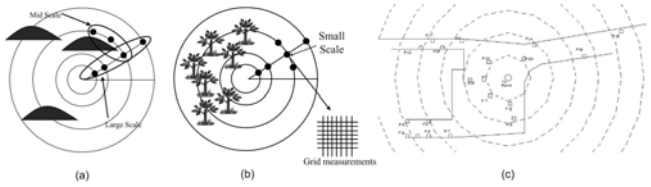

Fig. 1. Outdoor environments where the propagation measurement experiment was performed (a) hilly, (b) forest, (c) sub–urban

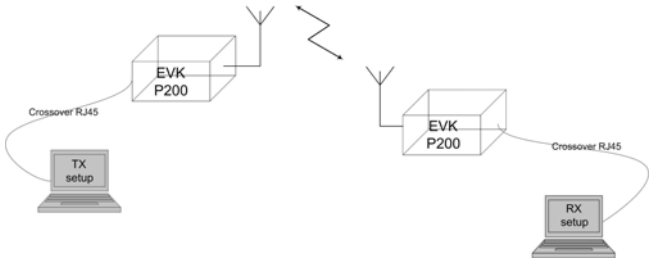

Fig. 2. Block diagram of the measurement set–up

In Section III, we describe the post–processing procedure adopted to obtain the desired channel parameters. For sake of brevity, we provide a detailed description of the results obtained in the forest scenario, while giving only few results for hilly and sub–urban environments. Conclusions are given in Section IV.

II. The Experiment Set–up

The three outdoor propagation scenarios, namely forest, hilly and sub–urban environments, are sketched in Fig. 1. For each environment, the position of the transmitter has been kept fixed, and different measurements have been taken at various positions of the receiver. In particular, for hilly and forest scenarios, such positions have been assumed on a set of concentric circles around the transmitter, in order to account for the effects of the Tx–Rx distance and azimuth angle as well. For the sub–urban scenario, positions have been chosen in order to explore various propagation conditions, at different distances and with different obstructions between Tx and Rx. Since cars and walls may play a major role in multipath generation in this latter context, particular care has been adopted to select measurement points. In addition, in order to account for the ground effect in analyzing path–loss and shadowing, the heights of both receiver and transmitter have been varied (0m, 1m and 1.5m) with respect to the ground. Moreover, for selected points in the forest scenario and for all points in the sub–urban one, position of the receiver has been moved on a 49 points grid. Adjacent points are separated by 15cm. The spacing yields significant sampling of spatial correlation, while the grid extension is large enough for providing relevant data for significant estimation of local Multipath Intensity Profile (MIP) statistics (obtained taking the average over the 49 local MIPs). In this case Tx and Rx have been fixed at 1m height with respect to the ground.

In detail, in the forest scenario, four distances have been considered, i.e. 10m, 25m, 40m and 60m, and the path–loss and shadowing statistics have been obtained over 36 measurement points (one point every 10° in the azimuth domain) for each distance; whereas the MIP profiles have been taken only in selected positions, thus collecting 9 MIPs for d=10m, d=25m and 4 and 3 MIPs for d=40m and d=60m, respectively. In the hilly terrain, three distances have been considered, i.e. 25, 45 and 70m, thus providing information for analyzing path–loss and shadowing over 16 measurement points (one point every 22.25° in the azimuth domain) for each distance. In the sub–urban scenario the Tx–Rx distance ranges from 10m to 52m, and in this case MIP profiles have been collected for each measurement point.

The technique adopted in this measurement campaign has consisted in probing the channel with very short pulses produced by the P200 Evaluation Kit (EVK P200): this consists of a pair of commercial UWB pulse transceivers, produced by Time–Domain Corporation (TDC) and designed to test the performance of Time Hopping (TH–) UWB systems and to provide basic features for UWB channel sounding. The setup has been completed by two laptops, one of which was connected to the receiver and used to collect and record sample waveforms (see Fig. 2). Each EVK can work both as a transmitter and as a receiver. When an EVK is used as a transmitter, it radiates a TH–UWB signal in the 3–6 GHz frequency band, in compliance to FCC limits. The receiver can acquire synchronization autonomously, without requiring a trigger reference signal. In detail [22], the EVK can capture the waveform of the received signal, by executing a virtual sampling with an equivalent sample time equal to 3ps. The acquired waveforms can be analyzed and visualized directly on the laptop connected to the Rx, by using a specific Performance Analysis Tool (PAT) developed by TDC. This allows to store the shape of the received pulse after propagating through the wireless medium, including both the channel characteristics and the transmitting and receiving antennas. So, in order to extract the channel impulse response, irrespective of the receiver and transmitter characteristics, the acquired samples have been off–line processed through a de–convolution technique known as CLEAN algorithm [19]. Figure 3 and Fig. 4 show the reference template used by the CLEAN algorithm to extract the echoes and the channel impulse response derived from a specific received signal in the forest scenario, respectively. The signal in Fig. 3 refers to the reference scenario in which the transmitter and the receiver are 1m apart, 1m above the ground and multipath propagation can be neglected. The signal in Fig. 4 refers to a large signal–to–noise ratio environment.

III. Data Post–Processing and Results

In this section we present a collection of results obtained from recorded waveforms. As described in [21], we separately analyze the effects of large, mid and small scale fading statistics. In particular, in this experiment, large–scale analysis is referred to variations of the (long–term) average signal strength with respect to the Tx–Rx distance (after averaging also with respect to azimuth). Mid–scale effects refer to variation of the received signal strength when Rx moves along a specific circle, thus exploring variations on the azimuthal plane for a given value of the Tx–Rx. Finally, small–scale effects refer to changes of e.g. MIPs induced by very small displacements of the receiver position. This occurs when the

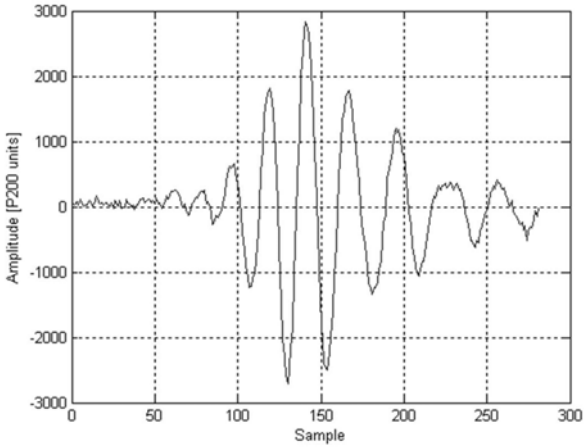

Fig. 3. Reference template used by the CLEAN algorithm

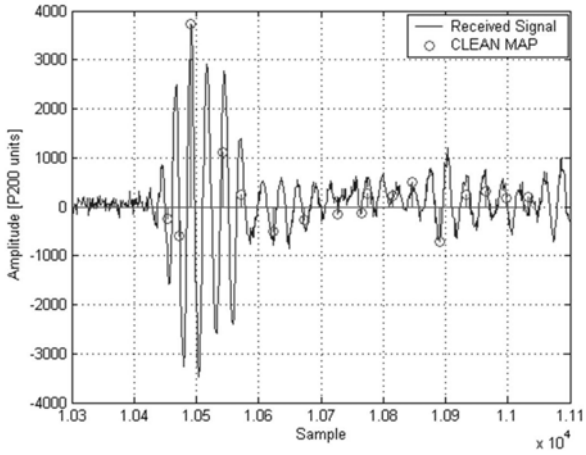

Fig. 4. Plots of the received signal and of the "cleaned" waveform

receiver is moved over the measurement grid for given values of azimuth and Tx–Rx distance.

A. Small–Scale Analysis

Small–Scale fading effects have been explored by using a procedure similar to the one described in [21]. In particular, these effects may cause differences between the received power delay profiles (PDP) at different points of the measurement grid. Here the MIP is defined as the average power delay profile (APDP) obtained by averaging the 49 local power delay profiles over each measurement grid. Each local PDP is obtained by quantizing the delay axis into bins of 2ns and integrating the received power in each bin.

In agreement with channel models derived in indoor scenarios (see e.g. [13] and [21]), a negative exponential decaying MIP has been obtained in forest and sub–urban scenarios, thus leading to MIP profiles with a decay constant depending on the specific measurement point. In addition, relevant statistical parameters related to time dispersion have been derived from the MIP, i.e. the Mean Excess delay, the RMS delay spread, the MIP slope related to the decay constant, the ratio between the first and the second bin and the number of multipath components with an amplitude within 10dB of the peak return.

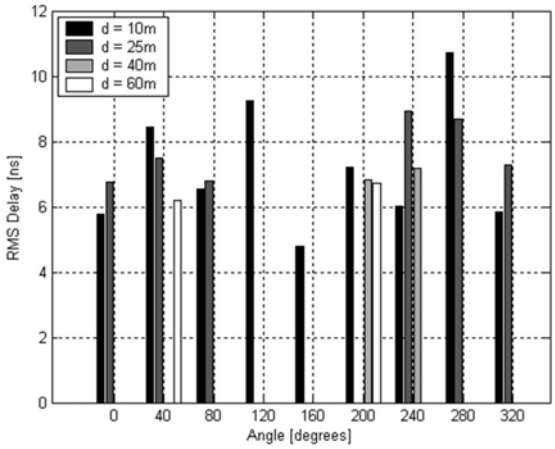

Fig. 5. RMS delay profile in the forest scenario

For sake of brevity, we only report in Fig. 5 the RMS delay with respect to the distance and the azimuth in the forest scenario. The general results obtained from this analysis can be summarized as follows for the forest scenario: i) Mean Excess and RMS delays exhibit a quite irregular behaviour with the azimuth and preliminary results show that at larger distances the mean excess delay slightly increases, while the RMS delay spread slightly decreases: this induces to consider that only a limited number of scatterers around the receiver contributes appreciably to the received signal. In any case, the RMS delay spread does not exceed 10ns: such a small value likely results, since trees and foliages mostly induce losses and diffusion, while they do not represent significant sources of delayed reflected paths; ii) the MIP slope is around -0.3 dB/ns at shorter distance, but decreases (sharper MIP decreases) at larger distances: this is in agreement with the RMS behaviour, since a decreasing delay spread is consistent with a more rapid MIP decreases which is in turn related to a less "dispersed" channel; iii) the drop of MIP amplitude from the first to the second echo shows an irregular behaviour as a function of the Tx–Rx distance and appears to be remarkably dependent on local propagation conditions. In any case, the second echo is almost one decade below the first echo; iv) the number of paths within 10dB remarkably increases at larger distances, even if, in this scenario, most energy is related only to few echoes (i.e. less than 8).

Finally, we have estimated the statistics of path amplitudes. In particular, the results of investigation reported here are restricted to the first echo in the MIP. These small–scale statistics can be characterized by fitting the received normalized energies in each bin (only the first bin here) to a distribution. The fitting has been attempted by resorting to typical one–sided distributions, namely negative exponential, Rayleigh, Gamma, and Log–Normal. The results clearly show that negative exponential and Rayleigh distributions provide a poor fitting of empirical data; on the contrary, Gamma and the Log–Normal models are able to provide a satisfactory fitting. An example of this fitting, along with its goodness assessed through the Kolmogorov–Smirnov test, is shown in Fig. 6.

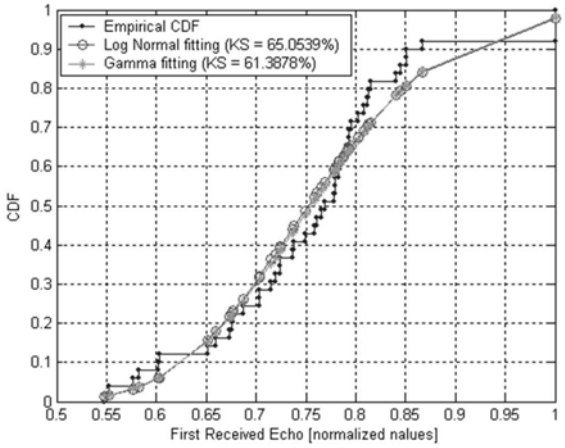

Fig. 6. Cumulative Distribution Function of small–scale effects

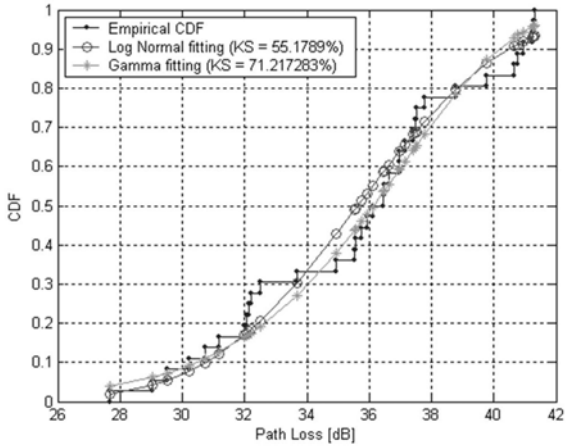

Fig. 7. Cumulative Distribution Function of mid–scale effects

B. Mid–Scale Analysis: Shadowing

Mid–Scale fading effects can be quantified by taking the standard deviation of the path–loss with respect to the azimuth position and for a fixed distance. Then, starting from similar results shown in Fig. 8 (discussed later) and from the average path–loss summarized in Table I, we have obtained the set of values listed in Table III for forest and hilly scenarios, with d=10m and d=25m.

TABLE I
PATH–LOSS: FOREST SCENARIO

TX–RX heights	d=10m	d=25m	d=40m
TXh=0m, RXh=0m	30.99dB	39.92dB	42.43dB
TXh=0m, RXh=1m	23.55dB	36.61dB	42.29dB
TXh=0m, RXh=1.5m	24.64dB	35.39dB	42.31dB
TXh=1m, RXh=0m	23.62dB	36.96dB	42.09dB
TXh=1m, RXh=1m	24.75dB	35.62dB	39.16dB
TXh=1m, RXh=1.5m	24.93dB	35.75dB	39.42dB
TXh=1.5m, RXh=0m	23.59dB	35.81dB	41.32dB
TXh=1.5m, RXh=1m	24.88dB	34.86dB	40.09dB
TXh=1.5m, RXh=1.5m	24.79dB	35.93dB	39.82dB

TABLE II
PATH–LOSS EXPONENT

TX–RX heights	Forest	Hilly	Sub–Urban
TXh=0m, RXh=0m	2.72dB/m	2.30dB/m	2.58dB/m
TXh=0m, RXh=1m	2.48dB/m	N.A.	N.A.
TXh=0m, RXh=1.5m	2.60dB/m	N.A.	N.A.
TXh=1m, RXh=0m	2.63dB/m	2.30dB/m	3.45dB/m
TXh=1m, RXh=1m	2.49dB/m	2.22dB/m	2.65dB/m
TXh=1m, RXh=1.5m	2.52dB/m	2.24dB/m	2.83dB/m
TXh=1.5m, RXh=0m	2.57dB/m	N.A.	N.A.
TXh=1.5m, RXh=1m	2.50dB/m	N.A.	N.A.
TXh=1.5m, RXh=1.5m	2.59dB/m	N.A.	N.A.

Moreover, we estimated first order distribution of mid–scale fluctuations and attempted matching with two typical laws (i.e. Log–Normal and Gamma). As an example, we report in Fig. 7 the empirical Cumulative Distribution Function (CDF) obtained from data shown in Fig. 8 along with the Log–Normal and Gamma best fit CDFs. The goodness of this matching has been assessed through the Kolmogorov–Smirnov (KS) test.

TABLE III
PATH–LOSS STANDARD DEVIATION

TX–RX heights	Forest (10m)	Forest (25m)	Hilly (25m)
TXh=0m, RXh=0m	4.93dB	2.11dB	5.06dB
TXh=0m, RXh=1m	4.68dB	3.50dB	N.A.
TXh=0m, RXh=1.5m	4.27dB	4.36dB	N.A.
TXh=1m, RXh=0m	5.23dB	3.61dB	6.12dB
TXh=1m, RXh=1m	4.59dB	3.75dB	1.53dB
TXh=1m, RXh=1.5m	3.93dB	3.71dB	0.61dB
TXh=1.5m, RXh=0m	3.74dB	4.87dB	N.A.
TXh=1.5m, RXh=1m	3.94dB	3.97dB	N.A.
TXh=1.5m, RXh=1.5m	4.13dB	3.87dB	N.A.

Although the agreement of measured data with the fitting curves is quite satisfactory, the above analysis can not lead yet to definitive results due to the small number of available measures.

C. Large–Scale Analysis: Path–Loss

For each measurement point, the path–loss has been estimated by taking the ratio between the mean value of the received signal (obtained by averaging the squared peak values of 12 acquired waveforms) and the squared peak value of the reference template shown in Fig. 3:

$$PL\left(d,\theta\right)=\frac{\frac{1}{12}\sum_{i=1}^{12}\left[s_i\left(t_{peak};d,\theta\right)\right]^2}{\left[s_{ref}\left(t_{peak}\right)\right]^2} \quad (1)$$

Figure 8 reports the values of path–loss in the forest scenario, as obtained for a fixed distance d=25m and various azimuth values. Tx and Rx are both 1m above the ground. Starting from (1), the path–loss is obtained by averaging with respect to the azimuth angle, for each distance. Table I summarizes the path–loss values obtained in the forest scenario. As suggested in Fig. 9 for the forest scenario, in order to identify a path–loss model, we have performed a linear fitting of estimated path losses at various Tx–Rx distances (e.g. the one in Table I): $PL\left(d\right)=10\alpha\log_{10}\left(d/d_0\right)$, with $d_0=1m$ denoting the reference distance and α the path–loss coefficient. The results obtained through this linear fitting are summarized in Table II for the analyzed scenarios (N.A. means the path–loss is not available for this configuration).

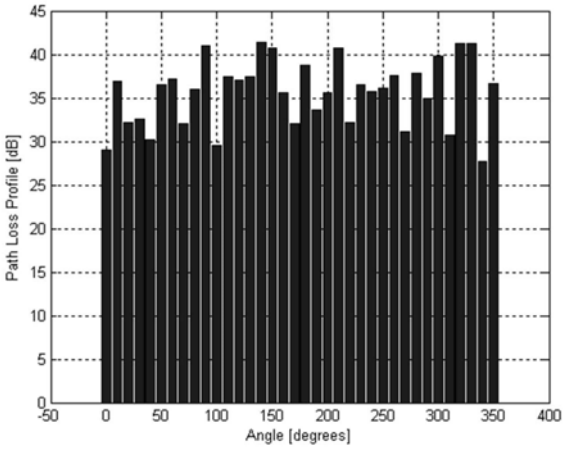

Fig. 8. Path–Loss profile with respect to the azimuth

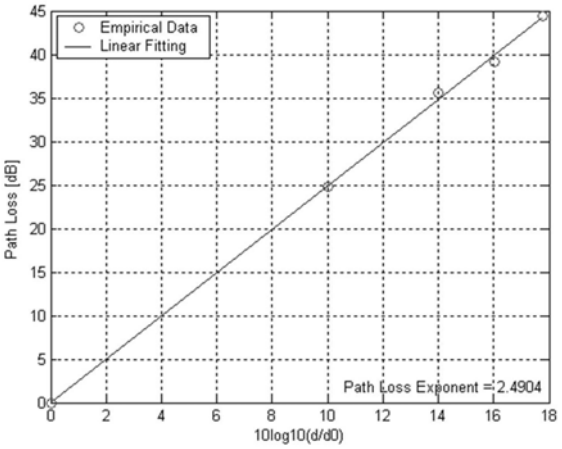

Fig. 9. Scatter plot of the large–scale attenuation versus the logarithm of the distance. The solid line represents the best fit using a linear path–loss model

IV. Conclusions and Future Work

An investigation of propagation behaviour of Ultra–Wide Bandwidth (UWB) signals in outdoor environments has been reported. With reference to a TDL channel model, results have been collected and statistical models have been derived for forest, hilly, and sub–urban scenarios. Some major remarks can be summarized as follows for the forest scenario: i) the average path–loss exponent is between 2.5 and 2.6; ii) mid–scale fluctuations and small–scale fading (first echo) can be described with a Log–Normal random variable; iii) MIP shows a negative exponential decay with a Mean Excess delay and a RMS delay belonging to the interval 1–4.5ns and 5–11ns, respectively; iv) the MIP slope and the ratio between the first and the second bin assume values in the intervals (-0.9)–(-0.27)dB/ns and 7–18dB, respectively; v) the number of multipath arrivals being within 10dB of the largest path arrival is always less than 8. These results induce to consider that the forest scenario is less time dispersive than indoor scenarios reported in the literature and that only a limited number of scatterers around the receiver contributes appreciably to the received signal. In addition, the results confirm that trees and foliages mostly induce losses and diffusion, while they do not represent significant sources of delayed reflected paths.

While companion contributions are dealing with more extensive results for hilly and sub–urban scenarios, as well as with outdoor–to–indoor propagation, further work is currently concerned with characterization of mid–scale fluctuations.

References

[1] R. A. Scholtz, *Multiple Access with Time Hopping Impulse Modulation*, MILCOM'93, Bedford, MA, October 11–14, 2003.

[2] Federal Communication Commission (FCC), *Revision of Part 15 of the Commission's Rules Regarding Ultra–Wideband Transmission Systems*, First Report and Order, ET Docket 98–153, February 2002.

[3] M. Z. Win and R. A. Scholtz, *Impulse radio: How it works*, IEEE Communication Letters, vol. 2, pp. 36-38, February 1998.

[4] M. Z. Win and R. A. Scholtz, *On the robustness of ultra–wide bandwidth signals in dense multipath environments*, IEEE Communication Letters, vol. 2, pp. 51-53, February 1998.

[5] M. Z. Win and R. A. Scholtz, *On the energy capture of ultra–wide bandwidth signals in dense multipath environments*, IEEE Communication Letters, vol. 2, pp. 145-147, 1998.

[6] D. Cassioli, M. Z. Win, F. Vatalaro, A. F. Molisch, *Performance of Low-Complexity Rake Reception in a Realistic UWB Channel*, IEEE Int. Conf. on Comm., 2002, vol. 2, pp. 763–767.

[7] V. S. Somayazulu, *Multiple Access Performance in UWB Systems using Time Hopping vs. Direct Sequence Spreading*, Intel Technology.

[8] R. Alesii, M. Di Renzo, F. Graziosi, F. Santucci, P. Tognolatti, *A Low–Complexity Receiver for Ultra Wide Band Communications*, IEEE Euro Electromagnetics Congress, 12–16 July 2004, Magdeburg, Germany.

[9] R. Alesii, F. Antonini, M. Di Renzo, F. Graziosi, F. Santucci, *Performance of a Chip–Time Analog Differential Receiver for UWB Systems in a Log–Normal Frequency–Selective Fading Channel*, Wireless Personal Multimedia Communications, 12–15 Sept. 2004, Abano Terme, Italy.

[10] R. T. Hoctor, H. W. Tomlinson, *An overview of delayed-hopped transmitted–reference RF communications*, Technique Information Series, G.E. Research and Development Center, January 2002.

[11] M. Ho, V. S. Somayazulu, J. Foerster, S. Roy, *A differential detector for an ultra-wideband communications system*, IEEE 55th Vehicular Technology Conference, Vol. 4, 6–9 May 2002, pp. 1896–1900.

[12] Y. L. Chao, R. A. Scholtz, *Optimal and Subotpimal Receivers for Ultra–wideband Transmitted Reference Systems*, IEEE Global Telecommunications Conference, GLOBECOM03, December 2003, pp. 759–763.

[13] J. Foerster, *Channel Modeling Sub–committee Report Final*, IEEE P802.15 Working Group for Wireless Personal Area Networks (WPANs), IEEE P802.15-02/490r1–SG3a, February, 2003.

[14] M. Z. Win, F. Ramirez–Mireles, R. A. Scholtz, M. A. Barnes, *Ultra–wide Bandwidth (UWB) Signal Propagation for Outdoor Wireless Communications*, IEEE 47th Veh. Tech. Conf., 1997, vol. 1, pp. 251–255.

[15] J. Foerster and Q. Li, *UWB Channel Modeling Contribution from Intel*, IEEE P802.15–02/279–SG3a.

[16] J. Kunisch and J. Pamp, *Radio Channel Model for Indoor UWB WPAN Environments*, IEEE P802.15–02/281–SG3a.

[17] S. Ghassemzadeh and V. Tarokh, *The Ultra–wideband Indoor Multipath Loss Model*, IEEE P802.15–02/282–SG3a, P802.15–02/283–SG3a.

[18] A. Molisch, M. Win, and D. Cassioli, *The Ultra–Wide Bandwidth Indoor Channel: from Statistical Model to Simulations*, IEEE P802.15–02/284–SG3a and IEEE P802.15–02/285–SG3a.

[19] S. M. Yano, *Investigating the Ultra–wideband Indoor Wireless Channel*, IEEE VTC 55th Vehicular Technology Conference, 2002, Vol. 3, pp. 1200–1204.

[20] J–M Cramer, R. Scholtz, M. Win, *Evaluation of an Indoor Ultra–Wideband Propagation Channel*, IEEE P802.15–02/286–SG3a and IEEE P802.15–02/325–SG3a.

[21] A. Molisch, M. Z. Win, D. Cassioli, *The Ultra–Wide Bandwidth Indoor Channel: from Statistical Model to Simulations*, IEEE Journal on Selected Areas in Communications, vol. 20, No. 6, August 2002, pp. 1247–1257.

[22] Time Domain Corporation, *www.timedomain.com.*

[23] A. F. Molisch et. al., *IEEE 802.15.4a channel model – final report*, IEEE 802.15-04-0662-01-04a, February, 2004.

[24] B. Kannan et. al., *Characterization of UWB Channels: Large–Scale Parameters for Indoor and Outdoor Office Environment*, IEEE 802.15–04–0383–00–04a, July 2004.

[25] B. Kannan et. al., *Characterization of UWB Channels: Small–Scale Parameters for Indoor and Outdoor Office Environment*, IEEE 802.15–04–0385–00–04a, July 2004.